# A theoretical model for investigating the structural dynamics of a rolling tyre

**Tania Simon**
Department of Mechanical Engineering
Politecnico di Milano
Via La Masa 1, 20156, Milano Italy
Email: tania.simon@mail.polimi.it

**Francesco Ripamonti**
Department of Mechanical Engineering
Politecnico di Milano
Via La Masa 1, 20156, Milano Italy
Email: francesco.ripamonti@polimi.it

**Roberto Corradi**
Department of Mechanical Engineering
Politecnico di Milano
Via La Masa 1, 20156, Milano Italy
Email: roberto.corradi@polimi.it

**Ivano La Paglia**
Department of Mechanical Engineering
Politecnico di Milano
Via La Masa 1, 20156, Milano Italy
Email: ivano.lapaglia@polimi.it

**Simone Baro**
Pirelli Tyres S.p.A.
Viale Piero e Alberto Pirelli 25, 20126, Milano, Italy
Email: simone.baro@pirelli.com

**ABSTRACT**

*The noise generated by the rolling tyre contributes significantly to the cars interior noise. This is caused by the tyre-road contact, and at low frequencies (0-500 Hz) is mostly transmitted inside the cockpit through the structure-borne transmission path. In support of the studies in this research field, an interpretative model of the tyre-wheel system accounting for the effects induced by the angular speed represents a useful tool. To this aim, we implemented an analytical model based on a flexible ring on an elastic foundation to analyse the dynamics of the tyre-wheel system, in both static and rotating configurations. We fine-tuned the parameters of the tyre based on data coming from an Experimental Modal Analysis of the static tyre. Particular attention has been paid to the system's free and forced responses, commonly analysed with the so-called cleat test. The results are discussed interpreting the behaviour in different reference systems.*

## 1 Introduction

For a long time, cars were used only as means of transport, but nowadays vehicles have become also places of leisure and work. Consequently, demands for car quality are increasing, particularly in terms of vibro-acoustic comfort. Indeed, excessive vehicle noise decreases interior sound quality and negatively affects people on-board by interfering with speech communication, work performance and sleep. The demand for improved vibro-acoustic comfort has led NVH (noise, vibration and harshness) performance to become an important design criterion in the development of new and better vehicles.

The car is subjected to three main noise and vibration sources: the powertrain, aerodynamics and tyre/road contact. Tyre noise is the major interior noise source when a vehicle moves at middling speed, especially on rough road [1]. This source is nowadays becoming more and more important, also thanks to the introduction of hybrid and electric power units, where powertrain excitation is reduced up to 15 dB at low speed [2].

The noise generated at the contact patch is transmitted inside the cabin both through the airborne and the structure-borne transmission paths. The first one contributes mainly at high frequency (>500 Hz) and is generally controlled through the optimal design of the cabin soundproofing. Being the results of the vibrations transmitted through the tyre structure to the hub and then through the suspension system and vehicle frame to the cabin, structure-borne noise instead contributes at low frequencies (0-500 Hz). In this case, the most promising way to reduce its influence is to act directly on the source [3, 4]. Among the different contributions, many authors, such as Wang and Bolton [5, 6, 7, 8], deepened the structural-acoustic coupling, with particular attention to tyre cavity mode. This resonance is typically located in the frequency range 200-220 Hz and results into a tonal contribution. A very effective solution to mitigate this disturbance is the introduction of sound absorbing materials (e.g foam liners) inside the tyre air volume, selectively increasing the damping of the acoustic mode [9].

As for the influence of tyre dynamics on structure-borne noise, both vehicle and tyre industries have invested in the development of predictive models [2, 10, 11, 12]. The models presented in the scientific literature can be divided in two main groups, finite element-based models and analytical models. The finite element (FE) models are computationally very expensive but allow accurate results and good correspondence with the real system. Lopez et al. [13] proposed the modelling of the vibrations of a rotating tyre up to 500 Hz. Their work is based on modal information extracted from an FE software, by means of which natural frequencies and mode shapes of a rolling tyre are computed. The authors compare the results with FE 2D and 3D models, being able to observe the asymmetry of the dispersion diagrams due to the effect of tyre rotation at frequencies above 100 Hz. Accurate FE based models have been developed by Nackenhorst [14] for the study of eigenvalues and eigenmodes of a stationary rolling tyre based on an Arbitrary Lagrange Eulerian (ALE) formulations: this combines the classical Lagrangian and Eulerian formulation allowing to obtain a model able to describe large deformations with high resolution. Starting from this theory, the weak formulation of the equations of motion have been developed: these are an integral form of the Partial Differential Equations (PDE), which are needed to formulate the FE method. Comparing the results of this author with others available in literature, an additional flux term is present in the equations of motion related to artificial boundaries coming from the ALE approach adopted. Diaz et al. [11] applied the ALE formulation previously presented in [14]. They compare the results from the numerical and the experimental approaches to study the effect of rotation on the tyre dynamics. A Finite Element model of a slick tyre as been developed through the software Abaqus 6.11.1.

This analysis suggested that in the non-rolling configuration, two waves are generated for each mode order, a regressive and a progressive wave travelling at the same speed. The superimposition of these two waves creates a standing wave. In the loaded rolling condition, the tyre is subjected to Coriolis acceleration, which makes the wave speed of the progressive and regressive waves to be different. This results in travelling mode shapes.

However, due to the complexity of the tyre-wheel system to be analysed, detailed FE models are not adequate for analysing this type of problem. Therefore, there is a need for a simpler model that can correctly present the physics of the tyre and simulate the dynamic response with a low computational effort. With this aim, analytical approaches have been introduced [15, 16]. A pioneer in the analytical modelling of a complex shape as the one of the thin ring is Soedel [17, 18]. Together with Huang [19], they analysed in detail the case of a rotating ring on elastic foundation and the effect of rotation on its dynamics. A thin ring of generic properties in the complete range of frequency bandwidth has been considered. For the calculation of the natural frequencies and mode shapes, a propagative wave solution is substituted in the equations of motion linearised around the steady state position. Solving the $n$th order equations, the bifurcation of the natural frequencies resulting from the introduction of the rotating speed is observed. For what concerns the eigenvectors, usually identifying the *modes* in the stationary condition, relevant differences from the ones defined in vibration analysis are obtained as they are function of time. Moreover, because of the ring rotating effect, they are neither standing nor rotating with the same speed $\Omega$ of the ring. The Huang-Soedel model is very interesting from the point of view of the natural response of the thin ring. However, it gives an erroneous result in terms of steady-state position when the thin ring is subjected to a stationary constant load: this results to be independent of the speed of rotation when no damping is taken into account. This is a consequence of the strain-displacement relation and the linearisation procedure, which lead to the Coriolis and centrifugal forces to cancel the pretensioning effect [21]. This detail is hardly mentioned by researchers except in [22] [23]; however, it is not so relevant if thin rings of very stiff materials such as steel are considered. Gong [12, 24] and Cooley [25] apply the theory of circular ring on elastic foundation on a real tyre case. The aim is to develop a tyre model suitable for the study of all aspects of in-plane dynamics and the vibration transmission properties. For what concerns the modelling, an approach similar to the one proposed by Soedel in [17, 18] is followed starting directly from the linearized equations of motion around the inflated tyre position. The only remarkable difference consists in adding an additional three degrees of freedom: in fact, the hub is considered as an independent element which is free to translate and rotate in the wheel plane. This fact allows a better understanding of the transmission properties on different boundary conditions. Once the natural frequencies and mode shapes are obtained, a parametric analysis investigating the extensional stiffness of the ring, the foundation stiffness, the rotating speed and the movement of the wheel is carried out.

More recently Metrikine et al. [21] proposed a revised model for the study of free vibrations of a thin rotating rings supported by an elastic foundation. In order to investigate the onset of instability phenomena associated to high rotating speeds in case of relatively stiff elastic bed, they introduced a through-thickness variation of the radial stress, emphasizing the stiffening resulting from the radial expansion due to the centrifugal load. In [26] they also proposed a higher-order formulation to include shear strain contribution and improve the study of the critical speeds.

Based on these ideas, we developed an analytical model of a flexible ring to reproduce the in-plane vibrating modes

of the non-rolling tyre and the behaviour in the case of rotating at constant speed. Attention is given to the study of the bifurcation effect of the natural frequencies caused by tyre rotation; for what concerns the system motion, its stationary or wave-like behaviour is investigated considering different reference systems. The validated model is tuned on a real tyre thanks to an Experimental Modal Analysis and is then used to simulate a *cleat test:* the tyre vibrational response is investigated focusing on the influence that rotation and damping have on tyre dynamics. From these results considerations are made on the interpretation of data coming from experimental cleat tests.

Differently from other literature models (see [12, 19]), in this paper the equilibrium position due to stationary constant loads is computed since its contribution is significant on elastic materials such as tyres, with an approach similar to [20]. The non-linear equations of motion are formulated considering also higher order terms in the strain-displacement relation. In a second step, the equilibrium position due to centrifugal load and inflation pressure is computed and the equations of motion are linearised around it. This procedure reduces the number of hypotheses the model relies on, making it more general and complete.

## 2 The Flexible Ring Theoretical Model

The model developed in this work is similar to the one presented in [19], in which the equations of motion of a steel flexible ring are derived. One remarkable assumption made in [19] is that the stress induced by the centrifugal force is independent of the radius variations and approximately equal to $\rho a^2 \Omega^2$, being $\rho$ the density per unit length, $a$ the mean radius and $\Omega$ the angular speed of the ring considered to be constant. As a consequence of the introduction of this assumption, the computational effort is reduced since the equations of motion turn out to be already linearised around the equilibrium position, which is unknown. In this paper some improvements are introduced to take into account the different behaviour of a tyre. Due to its high flexibility, the pre-tensioning of the ring subjected to uniform loads such as the inflation pressure and the centrifugal load needs to be correctly computed. Therefore, the non linear equations of motion are here derived firstly in the most general way. Then the equilibrium position due to uniformly distributed loads is evaluated and finally a linearization process is performed.

The tyre-wheel system is modelled as a thin circular ring supported on an elastic foundation as can be seen in Fig. 1. The in-plane dynamics of the tyre-wheel system is treated as a two-dimensional problem. The real system results from the assembly of three elements: the belt package, the sidewalls and the wheel. The first component, corresponding to the tread, is treated as a circular, thin, flexible ring made of a homogeneous elastic material. The ring is characterized by a mean radius in non-inflated conditions $a$ and a thickness $h$. The wheel is represented by an infinitely rigid and symmetric body characterized by its mass and moment of inertia. The belt package and the wheel are linked by the sidewalls, modelled as a massless elastic foundation composed of radial and circumferential springs ($k_r$, $k_\theta$) distributed along the entire ring circumference. The entire system rotates with an angular speed $\Omega$.

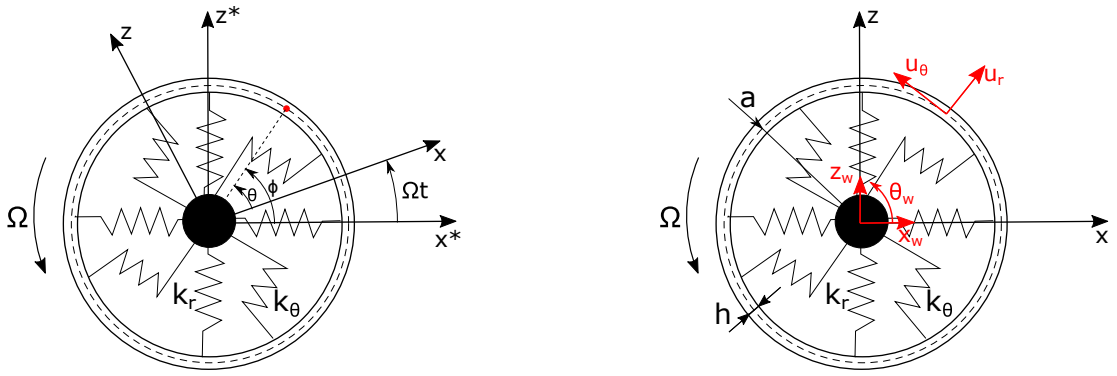


Fig. 1: Analytic model formulation of the thin flexible ring on elastic foundation: (a) the reference systems and (b) the independent coordinates

In Fig. 1.a, two types of reference systems are shown: the $x^* - z^*$ absolute (fixed in space) reference system and the $x - z$ system rotating with the wheel. The main reason for using two coordinate systems is that it is more convenient to study the vibration of the tyre in a rotating reference while the transmission to the car body in a fixed reference. The transformation equations that allow moving from one system to the other are:

$$x^* = xcos(\Omega t) - zsin(\Omega t) \tag{1a}$$

$$z^* = xsin(\Omega t) + zcos(\Omega t) \tag{1b}$$

$$\phi = \theta + \Omega t \tag{1c}$$

All the degrees of freedom (DOF) of the system are shown in Fig. 1.b. The circular flexible ring is characterized by infinite DOFs; to these, three DOFs (two displacements and one rotation) related to the wheel are added. Indeed, in the vertical plane, the wheel is characterized by three DOFs defined with respect to the rotating $x - z$ system: two translational (vertical $z_w$ and longitudinal $x_w$) and one rotational $\theta_w$. As for the tread, it can deform in radial and circumferential directions. The displacement components of the circular ring expressed in a rotating reference system are described by $\overline{u}_r$ in radial direction and $\overline{u}_\theta$ in circumferential direction (Eq. (2)). These quantities are formed by two contributions:

$$\overline{u}_r = u_r^o + u_r \tag{2a}$$

$$\overline{u}_\theta = u_\theta^o + u_\theta \tag{2b}$$

where $u_r^o$ and $u_\theta^o$ are time-independent terms indicating the equilibrium/steady-state position; $u_r$ and $u_\theta$ represent the dynamic oscillation around the equilibrium/steady-state position. The circumferential time-independent term $u_\theta^o$ is present only in the case a $\theta$-dependent load is applied. Only $\theta$-independent loading conditions are considered for the calculation of the free response.

The proposed modelling approach results in two Partial Differential Equations (PDE) of motion (relative to the ring's bending and circumferential deformation) and three Ordinary Differential Equations (ODE) (relative to the wheel). Hamilton's principle is applied to obtain the governing equations of the tyre-wheel system [27]. This approach requires the formulation of the energy functions: particular attention should be devoted to the potential energy $U$ of the thin flexible ring and the virtual work of the external forces applied on the ring in order not to neglect important terms for the steady state equilibrium position. For what concerns the first term, the general strain-displacement relations of the flexible ring have to be derived. Under the Euler-Bernoulli assumption for thin rings, in accordance with the frequency range of interest (limited to 0-300 Hz), the cross section of the ring remains plane and normal to the middle circumference after the deformation, so the only significant strain is in $\theta$ direction, while the transverse shear strain is negligible and the radial strain is null. The final expression of the strain-displacement relation in circumferential direction is:

$$\varepsilon_\theta = \frac{1}{a}\left(u_r + u_r^o + u_\theta^{'} + u_\theta^{'o}\right) + \frac{s}{a^2}\left(u_\theta^{'} + u_\theta^{'o} - u_r^{''} - u_r^{''o}\right) + \frac{1}{2a^2}\left[\left(u_r + u_r^o + u_\theta^{'} + u_\theta^{'o}\right)^2 + \left(u_\theta + u_\theta^o - u_r^{'} - u_r^{'o}\right)^2\right] \tag{3}$$

where $\square^{'}$ stands for the derivatives with respect to $\theta$ and $s$ is an auxiliary variable representing the radial distance from the middle circumference. The latter is adopted to compute the integral along the ring thickness, in between [-h/2; +h/2]. Second order non-linear terms in $\varepsilon_\theta$ are taken into account so as not to lose information related to the tension in the ring. In this way, the procedure adopted makes the model more specific with respect to the in-plane tyre dynamics.

the model is more complete and general than the ones present in literature since the number of hypothesis it is based on is reduced.

For what concerns the virtual work of the external forces applied on the ring, two generic forces $q_\theta(\theta,t)$ and $q_r(\theta,t)$ respectively applied in circumferential and radial direction are considered. Moreover, the contribution of the inflating pressure $p_o$ in radial direction should be considered. Its contribution is indeed fundamental for determining the correct equilibrium position and for properly investigating the tyre dynamics by accounting for the preload effect induced in the ring by the pressure itself. The final expression of the virtual work per unit width of the tyre yields:

$$\delta E_1 = \int_0^{2\pi} [q_\theta \delta u_\theta + (q_r + p_o)\delta u_r] a d\theta \tag{4}$$

being $\delta u_\theta$ and $\delta u_r$ the virtual displacements in circumferential and radial direction of a generic point.

The kinetic energy can be computed by considering the velocity of each infinitesimal arc element as a function of the radial and circumferential speed $\dot{u}_r$ and $\dot{u}_\theta$ expressed in the absolute reference system.

Once all the necessary energetic quantities have been obtained, Hamilton's Principle is applied for deriving the non-linear equations of motion of the tyre-wheel system (see Appendix A for details). In deriving them, the terms relative to the time-independent contribution, $u_\theta^o$ and $u_r^o$, are still present. These terms define in this specific case the steady-state displacements of the spinning ring in operating condition: because of the centrifugal forces and the inflation pressure, a pre-tensioning of the springs is present altering the position around which the dynamic response takes place. It is assumed that the spinning and inflating pressure effects are uniformly distributed along the ring, so $u_\theta^o$ and $u_r^o$ are supposed to be independent of the angular position. As a consequence, all the derivatives with respect to $\theta$ are zero, obtaining:

$$\begin{cases} (u_r^o)^3\left(\frac{K}{2a^4}\right)+(u_r^o)^2\left(\frac{3K}{2a^3}\right)+(u_\theta^o)^2\left(\frac{K}{2a^3}\right)+u_r^o(u_\theta^o)^2\left(\frac{K}{2a^4}\right)+u_r^o(-\rho h\Omega^2+k_r+\frac{K}{a^2})-\rho ha\Omega^2-p_o=0 \\ (u_\theta^o)^3\left(\frac{K}{2a^4}\right)+(u_r^o)^2u_\theta^o\left(\frac{K}{2a^4}\right)+u_r^ou_\theta^o\left(\frac{K}{a^3}\right)+u_\theta^o(-\rho h\Omega^2+k_\theta)=0 \end{cases} \tag{5}$$

where $K=Eh$, $D=Eh^3/12$ are respectively the axial and bending stiffness per unit width of the ring. From the second equation we can immediately notice that one possible solution is $u_\theta^o=0$. This is also the only acceptable solution for this case because of the axial-symmetry of the problem. The first cubic algebraic equation has been numerically solved to find the three possible solutions. We noticed that two out of three are out of the acceptability range. Consequently, only one couple $(u_r^o,0)$ defining the steady-state position is obtained. From the previous system of equations we observed that the steady-state radial displacement $u_r^o$ varies with the speed of rotation. In particular, the higher the speed of rotation, the bigger the radial displacement. In the same way, $u_r^o$ varies also with the inflation pressure, where this effect is always present, also in the non-rotating case. Therefore, a steady-state radial displacement will always appear both in the rotating and non-rotating cases.

The formulation of the steady state position makes the model more general: in [19] the equations of motion are already linearized around a constant and assigned uniform equilibrium position. By means of the complete formulation, the model proposed in this paper can be used also for non-uniform pre-tensioning forces whose analytical expression is known (such as the tyre pressed on the road).

Once the steady-state position of the spinning circular ring has been found, the equations of motion can be linearised around this position and the expressions representing both radial and circumferential perturbed motion are derived.

**PDE tyre: radial direction**

$$\begin{aligned} &-\rho h(-\ddot{u}_r+2\dot{u}_\theta\Omega+u_r\Omega^2)+\frac{K}{a^2}(u_\theta'+u_r)+\frac{D}{a^4}(u_r^{IV}-u_\theta''')+\frac{K}{2a^4}(u_r^o)^2(3u_r+4u_\theta'-u_r'')+ \\ &+\frac{K}{a^3}u_r^o(3u_r+4u_\theta'-u_r'')+k_r(u_r-x_w cos\theta-z_w sin\theta)=q_r \end{aligned} \tag{6}$$

**PDE tyre: circumferential direction**

$$
\begin{aligned}
&-\rho h(-\ddot{u}_\theta - 2\dot{u}_r\Omega + u_\theta\Omega^2) - \frac{K}{a^2}(u_\theta'' + u_r') - \frac{D}{a^4}(u_\theta'' - u_r''') - \frac{K}{2a^4}(u_r^o)^2(-u_\theta + 4u_r' + 3u_\theta'') - \\
&+ \frac{K}{a^3}u_r^o(-u_\theta + 4u_r' + 3u_\theta'') + k_\theta(u_\theta + x_w sin\theta - z_w cos\theta - a\theta_w) = q_\theta
\end{aligned}
\tag{7}
$$

The same procedure followed for the tyre is applied also on the wheel, and the governing linearized equations are obtained. These are important for investigating the transmission properties of the vibrations inside the cockpit.

**ODE wheel:**

$$
-m(-\ddot{x}_w + 2\dot{z}_w\Omega + x_w\Omega^2) + a\pi(k_\theta + k_r)x_w + a\int_0^{2\pi}[k_\theta u_\theta sin\theta - k_r u_r cos\theta]d\theta = f_x \tag{8}
$$

$$
-m(-\ddot{z}_w - 2\dot{x}_w\Omega + z_w\Omega^2) + a\pi(k_\theta + k_r)z_w + a\int_0^{2\pi}[-k_\theta u_\theta cos\theta - k_r u_r sin\theta]d\theta = f_z \tag{9}
$$

$$
I_r\ddot{\theta}_w + 2\pi k_\theta a^3\theta_w - a^2\int_0^{2\pi}k_\theta u_\theta d\theta = T_y \tag{10}
$$

where $f_x$ and $f_z$ represent the forces in vertical and horizontal direction applied at the hub and $T_y$ the torque.

## 3 Tyre Vibration - Free Response Solution

The equations of motion introduced in Section 2 can be used to study the free response of the system. The PDE equations of motion of the flexible ring (Eq. (6) and Eq. (7)) under the assumption of fixed hub are considered. This is a common experimental condition for tyres in indoor tests on rigid corners. Due to the geometry of the tyre, the displacements of the ring in radial and tangential direction must be periodic functions of the angular coordinate. Furthermore, assuming a time harmonic dependency $e^{i\omega t}$, a wave propagative solution of the following form is considered:

$$
u_r(\theta,t) = A_n e^{in\theta}e^{i\omega_n t} \tag{11a}
$$

$$
u_\theta(\theta,t) = B_n e^{in\theta}e^{i\omega_n t} \tag{11b}
$$

where $n$ is an integer representing the mode order (being $2\pi/n$ the period with respect to the angular position $\theta$). By taking the required derivatives and substituting in the equations of motion, the following matricial form can be obtained:

$$\begin{bmatrix} M_{11} & M_{12} \\ M_{21} & M_{22} \end{bmatrix} \begin{bmatrix} A_n \\ B_n \end{bmatrix} = 0 \tag{12}$$

with:

$$\begin{aligned}
M_{11} &= -\rho h\omega^2 - \rho h\Omega^2 + \frac{K}{a^2} + \frac{D}{a^4}n^4 + \frac{3K}{2a^4}(u_r^o)^2 + \frac{K}{2a^4}(u_r^o)^2 n^2 + \frac{3K}{a^3}u_r^o + \frac{K}{a^3}u_r^o n^2 + k_r \\
M_{12} &= i\left(-2\rho h\Omega\omega + \frac{K}{a^2}n + \frac{D}{a^4}n^3 + \frac{4K}{2a^4}(u_r^o)^2 n + \frac{4K}{a^3}u_r^o n\right) \\
M_{21} &= -M_{12} \\
M_{22} &= -\rho h\omega^2 - \rho h\Omega^2 + \frac{D}{a^4}n^2 + \frac{K}{a^2}n^2 + \frac{K}{2a^4}(u_r^o)^2 + \frac{3K}{2a^4}(u_r^o)^2 n^2 + \frac{K}{a^3}u_r^o + \frac{3K}{a^3}u_r^o n^2 + k_\theta
\end{aligned}$$

The forcing terms $q_r$ and $q_\theta$ are set to zero to investigate the system free motion. In order to get a non-trivial solution, the determinant of the coefficient matrix in Eq. (12) must be zero. This would result in the following $4^{th}$ order polynomial characteristic equation:

$$a_3\omega_n^4 + a_2\omega_n^2 + a_1\omega_n + a_0 = 0 \tag{14}$$

with:

$$\begin{aligned}
a_3 = {} & \rho^2 h^2 \\
a_2 = {} & -\rho h\left(-\rho h\Omega^2 + \frac{D}{a^4}n^2 + \frac{K}{a^2}n^2 + \frac{K}{2a^4}(u_r^o)^2 + \frac{3K}{2a^4}(u_r^o)^2 n^2 + \frac{K}{a^3}u_r^o + \frac{3K}{a^3}u_r^o n^2 + k_\theta\right) + \\
& -\rho h\left(-\rho h\Omega^2 + \frac{K}{a^2} + \frac{D}{a^4}n^4 + \frac{3K}{2a^4}(u_r^o)^2 + \frac{K}{2a^4}(u_r^o)^2 n^2 + \frac{3K}{a^3}u_r^o + \frac{K}{a^3}u_r^o n^2 + k_r\right) + \\
& -4\rho^2 h^2\Omega^2 \\
a_1 = {} & 4\rho h\Omega\left(\frac{K}{a^2}n + \frac{D}{a^4}n^3 + \frac{4K}{2a^4}(u_r^o)^2 n + \frac{4K}{a^3}u_r^o n\right) \\
a_0 = {} & \left(-\rho h\Omega^2 + \frac{K}{a^2} + \frac{D}{a^4}n^4 + \frac{3K}{2a^4}(u_r^o)^2 + \frac{K}{2a^4}(u_r^o)^2 n^2 + \frac{3K}{a^3}u_r^o + \frac{K}{a^3}u_r^o n^2 + k_r\right) \cdot \\
& \left(-\rho h\Omega^2 + \frac{D}{a^4}n^2 + \frac{K}{a^2}n^2 + \frac{K}{2a^4}(u_r^o)^2 + \frac{3K}{2a^4}(u_r^o)^2 n^2 + \frac{K}{a^3}u_r^o + \frac{3K}{a^3}u_r^o n^2 + k_\theta\right) + \\
& + \left(\frac{K}{a^2}n + \frac{D}{a^4}n^3 + \frac{4K}{2a^4}(u_r^o)^2 n + \frac{4K}{a^3}u_r^o n\right)\left(-\frac{D}{a^4}n^3 - \frac{K}{a^2}n - \frac{4K}{2a^4}(u_r^o)^2 n - \frac{4K}{a^3}u_r^o n\right)
\end{aligned}$$

The solutions of Eq. (14) are the characteristic polynomial roots corresponding to the $n$th wave-like motion of the ring, being $n$ an integer number in between $[-\infty;+\infty]$. In general, for each integer value of $n \neq 0$, there are four characteristic poly-

nomial roots $k = 1,2,3,4$ (two positive and two negative). The magnitudes of the positive ones are the circular frequencies associated to a regressive wave-like motion, while the magnitudes of the negative ones are the circular frequencies associated to a progressive wave-like motion. Noting that the coefficient $a_1$ depends on the tyre-wheel angular speed $\Omega$, in the specific case where the ring is not rotating ($\Omega = 0$) the solutions to Eq. (14) come in couples: this means that the circular frequencies $\omega_{n,1}$, $\omega_{n,2}$, $\omega_{n,3}$, $\omega_{n,4}$ are opposite in sign two by two ($\omega_{n,2} = -\omega_{n,1}$). Otherwise, if the ring is rotating ($\Omega > 0$), four distinct circular frequencies $\omega_{n,1}$, $\omega_{n,2}$, $\omega_{n,3}$, $\omega_{n,4}$ can be found resulting from the bifurcation caused by the Coriolis acceleration $2\rho h\Omega\omega$ present in the extra-diagonal terms of matrix M. Two circular frequencies, lower in magnitude, are called inextensional, while the other two, higher in magnitude, are called extensional [19]. Since the aim of this paper is to investigate the 0-300 Hz frequency range, particular attention will be paid to the inextensional results. Once the characteristic polynomial roots are known, the associated eigenvectors can be computed through Eq. (12). Since the matrix M has been imposed to be singular, the two corresponding equations are no longer independent. A normalized eigenvector is therefore sought, where one of the coefficients $A_n$ or $B_n$ is imposed and the remaining one is computed by solving one of the tyre equations.

In Tabs. 1 and 2 the relationships between the different characteristic polynomial roots and eigenvectors are presented for varying angular speed $\Omega$ and order $n$. In Tabs. 1 and 2 first row the non-rotating case is shown where the two couples of characteristic polynomial roots are equal in modulus. In the case $n \leq -1$ the couples are still present, but roots are inverted ($\omega_{-n,1} = -\omega_{n,1}$). Looking at the eigenvector, we can notice that for each couple $k = 1,2$ or $k = 3,4$ and for a given order $n$ they are equal in sign. However, comparing the cases $n \geq 1$ and $n \leq -1$ for the same $k$, we can see that the term relative to the circumferential displacement changes in sign. These last two properties are very important for realizing a real valued wave-like motion (the so-called *standing wave*).

In Tabs. 1 and 2 second row, an angular speed different from zero is considered and we can see that the characteristic polynomial roots now are all different. Relating to the case $n \leq -1$, the same considerations on the signs done for the $\Omega = 0$ case can be applied.

From now on, in all the analyses the characteristic polynomial roots and eigenvector components will be written with the explicit sign.

| **Conditions** | | **Inextensional** | | **Extensional** | |
|---|---|---|---|---|---|
| **Ω** | **n** | **k=1** | **k=2** | **k=3** | **k=4** |
| $\Omega = 0$ | $n \geq 1$ | $\omega_{n,1}$ | $-\omega_{n,1}$ | $\omega_{n,3}$ | $-\omega_{n,3}$ |
| | $n \leq 1$ | $-\omega_{n,1}$ | $\omega_{n,1}$ | $-\omega_{n,3}$ | $\omega_{n,3}$ |
| $\Omega \neq 0$ | $n \geq 1$ | $\omega_{n,1}$ | $-\omega_{n,2}$ | $\omega_{n,3}$ | $-\omega_{n,4}$ |
| | $n \leq 1$ | $-\omega_{n,1}$ | $\omega_{n,2}$ | $-\omega_{n,3}$ | $\omega_{n,4}$ |

Table 1: Relation between characteristic polynomial roots in the non rotating ($\Omega = 0$) and rotating ($\Omega \neq 0$) case; notice that all signs are explicit

| Conditions | | Inextensional | | Extensional | |
|---|---|---|---|---|---|
| **Ω** | **n** | **k=1** | **k=2** | **k=3** | **k=4** |
| $\Omega = 0$ | $n \geq 1$ | $[1, iB_{n,1}]$ | $[1, iB_{n,1}]$ | $[1, -iB_{n,3}]$ | $[1, -iB_{n,3}]$ |
| | $n \leq -1$ | $[1, -iB_{n,1}]$ | $[1, -iB_{n,1}]$ | $[1, iB_{n,3}]$ | $[1, iB_{n,3}]$ |
| $\Omega \neq 0$ | $n \geq 1$ | $[1, iB_{n,1}]$ | $[1, iB_{n,2}]$ | $[1, -iB_{n,3}]$ | $[1, -iB_{n,4}]$ |
| | $n \leq -1$ | $[1, -iB_{n,1}]$ | $[1, -iB_{n,2}]$ | $[1, iB_{n,3}]$ | $[1, iB_{n,4}]$ |

Table 2: Relation between eigenvectors in the non rotating ($\Omega = 0$) and rotating ($\Omega \neq 0$) case; notice that the signs and the imaginary unit are explicit

## 4 Model Tuning and Validation

The model developed was first validated based on data of the steel ring introduced in [19]. High correspondence of the natural frequencies was obtained confirming that the approach proposed in this paper and based on a reduced number of hypothesis is complete and general.

Subsequently, the model was tuned on a real tyre based on results coming from an experimental campaign performed in Politecnico di Milano laboratories. This activity aims at identifying the modal dynamic properties of the tyre in order to validate the developed model. The test set-up and the measurement system were entirely designed during this research and an Experimental Modal Analysis (EMA) was performed to identify the natural frequencies and mode shapes in the 0-300 Hz frequency band.

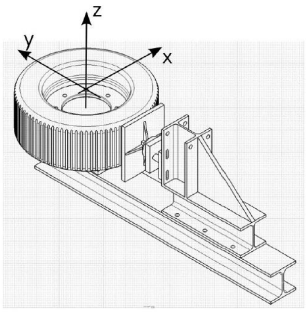


(a)

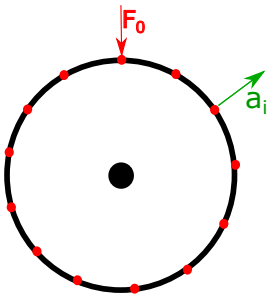


(b)

(c)

(d)

Fig. 2: Experimental Modal Analysis (EMA) setup at the Mechanical Department of Politecnico di Milano: (a) design of the test bench; (b) summary sketch of excitation and measuring points; (c) picture of accelerometers placed in radial direction; (d) picture of a detail of the excitation point

The complete experimental set-up is depicted in Fig. 2. The reference tyre (tyre model 225/55R17) is mounted on a commercial wheel with the external side upwards. The entire structure is rigidly fixed by means of clamps to the suspended foundation underneath. The tyre is excited by an electro-dynamic shaker TiraVIB TV5500. The excitation point was preloaded with 50 $N$ to avoid the detaching of the leading stinger from the tyre. In between the stinger and the tyre, a piezoelectric loading cell was installed to measure the force entering the system (Fig. 2.d ). The response of the system was measured sticking 13 piezo-electric accelerometers (PCB333B30) on the external part of the tyre with cyanoacrylate and 2 PCB Piezotronics conditioning system 483C50 with 8 channels (Fig. 2.c). To increase the number of measuring points and avoid any kind of mass load effect, the 13 accelerometers were uniformly distributed along the circumference and then rotated. Given a 5-degree measuring grid, a total of 72 measuring positions were obtained corresponding to 6 configurations. Only one accelerometer out of the 13 available was kept fixed as a reference to verify that no relevant differences in the tyre dynamic response was obtained by the change in sensor positioning. The signal was acquired with a sampling frequency of 2 kHz for a time of 250 seconds.

At the post processing stage, the frequency response function (FRFs) between each accelerometer signal and the shaker force were computed, applying the $H_1$ FRF estimator and 10 averages to reduce the background noise. Furthermore, the modal identification procedure was performed, thus providing in output the natural frequencies, the non-dimensional damping ratios and the mode shapes. The software adopted ( [28], [29]) is based on two steps:

1. The first, based on the LSCE algorithm (Least Squares Complex Exponentials), allows the identification of the poles of the system on the frequency range of interest. It evaluates the stability and provides a first attempt data for the natural frequencies and the damping ratios.
2. The second step consists in the classical FRF-based curve fitting method: according to the idea of modal superposition, the measured FRFs are fitted with an analytical model consisting of a series of second order dynamic systems. Least squares minimisation operates in a user-defined frequency band which includes a certain number of vibration modes: a limited variation of their natural frequencies and damping ratios with respect to the previous LSCE estimates is allowed. To reach suitable curve-fit, high and low frequency residuals are added to the resonant modes so as to account for the contribution of the modes not included in the selected frequency band.

The final outputs are the modal parameters (i.e. natural frequencies, damping ratios and mode shapes) of the system included in the frequency band of interest. In Fig. 3, as an example, the comparison between the experimental (dashed line) and the identified (solid line) FRF (inertance) between the force applied and the acceleration measured in node 20 is presented. Tab. 3 summarises the first seven natural frequencies and the damping ratios identified for the considered unloaded tyre.

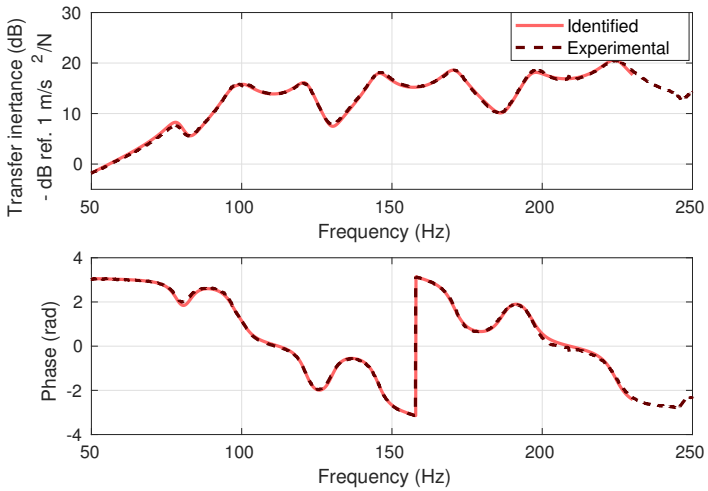


Fig. 3: Frequency Response Function (FRF) between the radial force and the radial acceleration measured at node 20 (100°): comparison between the measured and the identified transfer inertance

| **Mode (n)** | **Frequency (Hz)** | **Damping ratio ξ (-)** |
|---|---|---|
| 1 | 78,73 | 0,039 |
| 2 | 100,31 | 0,033 |
| 3 | 121,40 | 0,024 |
| 4 | 145,45 | 0,022 |
| 5 | 170,78 | 0,021 |
| 6 | 196,52 | 0,020 |
| 7 | 224,40 | 0,018 |

Table 3: Identified natural frequencies and damping ratios (unloaded tyre)

Being the EMA completed, the natural frequencies and corresponding mode shapes can be used to tune the analytical model. The main variables of the theoretical model influencing the system dynamics are:

- the density per unit width $\rho h$
- the radial stiffness of the elastic bed $k_r$
- the circumferential stiffness of the elastic bed $k_\theta$
- the axial stiffness of the circular ring $K$
- the bending stiffness of the circular ring $D$

Through an optimization algorithm these parameters are varied in order to match the experimental results. In particular, considering the characteristic polynomial presented in Section 3 (Eq. (14)), the experimental natural frequencies are imposed, while the coefficients of the polynomial are unknown since they depend on the parameters to be optimized. Throughout the

optimization, a relation is introduced between the axial stiffness of the tyre $K$ and the radial stiffness of the elastic bed $k_r$ resulting from the equilibrium position equation in radial direction (Eq. (5)): indeed, there is a strong relation between the inflation pressure and the elastic properties of the thin ring and the elastic bed. As a result, the condition:

$$K = \frac{\rho h \Omega^2 u_r^o + \rho h a \Omega^2 - k_r u_r^o + p_o}{\frac{(u_r^o)^3}{2a^4} + \frac{3(u_r^o)^2}{2a^3} + \frac{u_r^o}{a^2}} \tag{16}$$

is included reducing the total number of variables. Being $FUN$ the function to be minimized, the operator computes:

$$\min FUN = \left[ \min \sum_{n=1}^{7} Fun_n^2 \right] \tag{17}$$

where:

$$Fun_n = a_3^n \omega_n^4 + a_2^n \omega_n^2 + a_1^n \omega_n + a_0^n = 0 \tag{18}$$

and $a_j^n$ are the coefficients depending on the parameters to be optimized ($\rho h$, $k_r$, $k_\theta$, $D$) varying with the order $n$, while $\omega_n$ is the natural frequency desired coming from experimental analysis.

The non-linear least square problem is solved with a trust region reflective algorithm, which identifies local minima. Therefore, to guide the minimization, reliable initial conditions have to be assigned (coming from FEA). Moreover, a constraint minimization is performed. A sensitivity analysis has been carried out to test the vibration mode dependency on model parameters. Thus, upper and lower bounds of the constraints have been defined. The algorithm returns a vector containing the optimized parameters. Tab. 4 summarizes the outcomes of the optimization algorithm obtained by using the measured mean radius $a = 0.33$ m.

| **Parameter** | **Optimized Value** |
|---|---|
| $\rho h$ (kg m$^{-2}$) | $19,69$ |
| $k_\theta$ (N m$^{-3}$) | $6,56 \cdot 10^5$ |
| $k_r$ (N m$^{-3}$) | $8,27 \cdot 10^6$ |
| $K$ (N m$^{-1}$) | $2,52 \cdot 10^7$ |
| $D$ (N m) | $7,45$ |

Table 4: Optimal parameter values

In Fig. 4 the correspondence between the experimental and the analytical natural frequencies and mode shapes, computed from the model at $\Omega = 0$ rad/s after the optimization process, is shown in terms of scatterplot (Fig. 4.a) and MAC (Modal Assurance Criterion) (Fig. 4.b). High levels of accuracy are reached. The frequencies resulting from the updated model show variations with respect to the experimental ones lower than 1%. The only exception is represented by the first mode, for which a difference of 3 Hz is obtained. For what concerns the modes, a correspondence greater than 80% (MAC$>0.8$) is shown for all the seven modes.

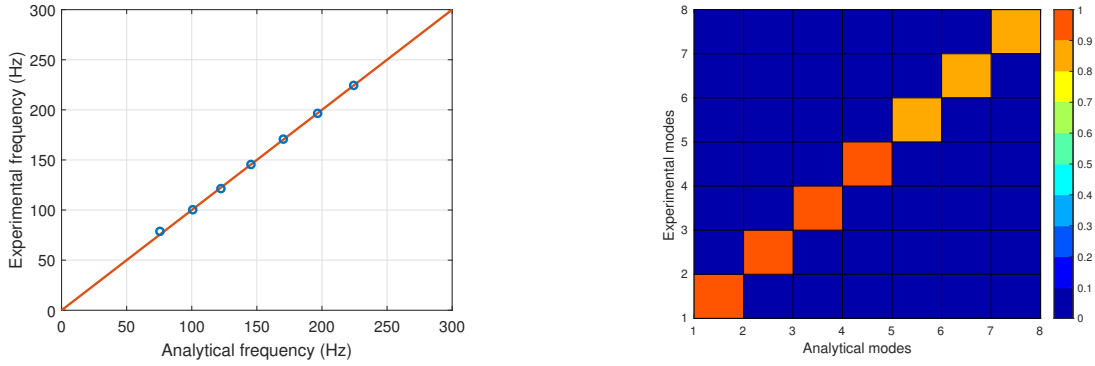


(a) (b)

Fig. 4: Comparison between the identified and the analytical modal parameters of the inflated tyre at $\Omega = 0$ rad/s: (a) scatterplot of the natural frequencies; (b) Modal Assurance Criterion (MAC) of the vibration modes

The model parameters, identified in static conditions and providing accurate results both in terms of natural frequencies and vibration modes, will be assumed constant also in the rolling tyre condition for the considered range of speed.

## 5 Results and Discussion

Hereafter we present the results of the model tuned on the data of Tab. 4 (tyre model 225/55R17). First of all, the free response of the tyre in the rotating and non-rotating cases is analysed starting from the considerations made in Section 3. Then the same response in different reference systems is evaluated and considerations are made on the stationarity of the generated wave. Finally, the tyre inertance due to a single impulsive radial load is calculated too.

### 5.1 The Free Response of the Undamped Tyre

Let us consider the non-rotating and rotating cases separately. According to the relationships presented in Tabs. 1 and 2 first row, in the non-rotating case ($\Omega = 0$) the expressions for the displacements in radial and circumferential directions can be obtained by considering only the inextensional solutions and superimposing $k = 1$ and $k = 2$:

$$u_{r,tot} = 2cos(n\theta + \omega_{n,1}t) + 2cos(n\theta - \omega_{n,1}t) \tag{19a}$$

$$u_{\theta,tot} = -2B_{n,1}sin(n\theta + \omega_{n,1}t) - 2B_{n,1}sin(n\theta - \omega_{n,1}t) \tag{19b}$$

By using Prosthaphaeresis trigonometric formulae, Eq. (19) can be rewritten as:

$$u_{r,tot} = 4cos(n\theta)cos(\omega_{n,1}t) \tag{20a}$$

$$u_{\theta,tot} = -4B_{n,1}sin(n\theta)cos(\omega_{n,1}t) \tag{20b}$$

The waves in Eq. (20) have been rewritten as the product of two sinusoidal functions. The first, depending only on the angular position $\theta$, represents the mode shape while the second acts as a time modulating function. Thanks to the previous mathematical passages, we can assert that a standing wave occurs at the ring natural frequencies in the non-rotating case. This is the result of the superposition of the two waves propagating with the same speed $c = \omega/n$ in opposite directions.

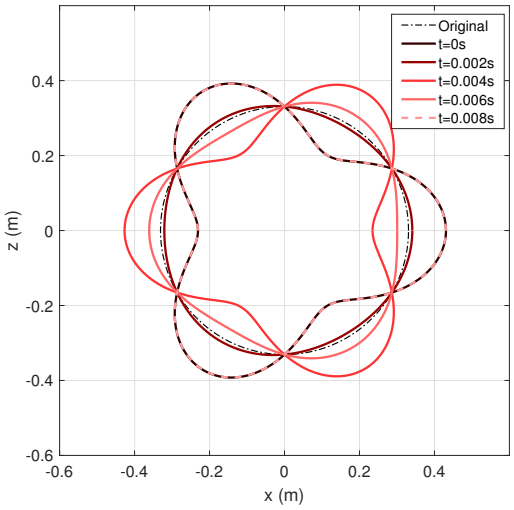


Fig. 5: Free response, ($u_{r,tot}$), of the flexible ring resulting from the superimposition of the progressive and regressive waves at $n = 3$ and $\Omega = 0$ rad/s. Different time lapse in the rotating reference system (in this case equal to the absolute one)

From the sequence in Fig. 5 representing the ring radial displacement ($u_{r,tot}$) at different time instants, we can see that, by summing the two waves, a pulsing behaviour takes place, clearly showing the nodes and antinodes of the standing wave. The curves at $t = 0$ s and $t = 0.008$ s representing the beginning and end of a cycle respectively, are perfectly superimposed. The same reasoning can be applied to any order $n$, for which the two resulting waves will always superimpose to realize a standing wave.

When the tyre is rotating ($\Omega \neq 0$), coefficient $a_1$ in Eq. (14) is not null and four different circular frequencies $\omega_{n,1}$, $\omega_{n,2}$, $\omega_{n,3}$, $\omega_{n,4}$ are obtained. With respect to the non-rotating case, one frequency is increased while the other is decreased. The values, which in the non-rotating case are coincident, here are separated and the increment/decrement depends on the angular speed and on the order considered. This behaviour is called bifurcation and is a result of the Coriolis effect $2\rho h\Omega\omega$ present in the extra-diagonal terms of matrix M (Eq. (12)).

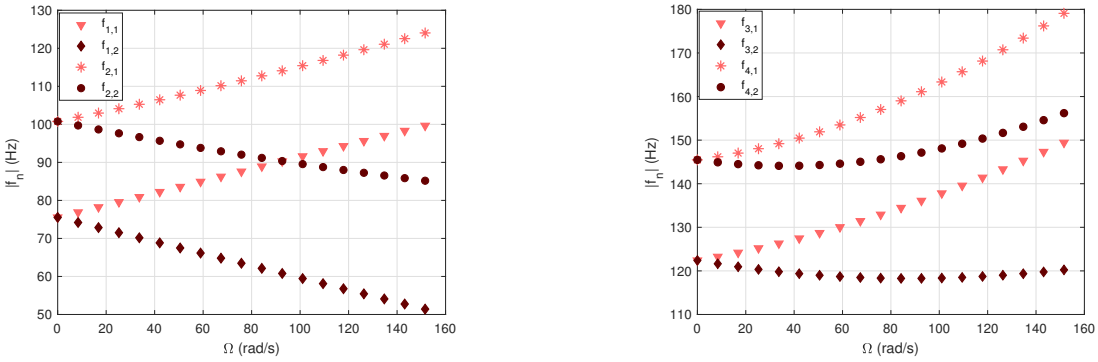


(a) (b)

Fig. 6: Natural frequencies of the flexible ring analytical model as a function of the rotating speed. Bifurcation effect of the inextensional frequencies ($f_n = \omega_n/2\pi$) for (a) n=1 and n=2; (b) n=3 and n=4

Fig. 6 shows the bifurcation of the inextensional frequencies due to the rotational speed of the tyre. For each bifurcation, the higher frequency lines are associated to a regressive wave-like motion, while the lower frequency lines are associated to the progressive wave-like motion (see Eq. (21)).

We can see that for $n = 1$ the bifurcation is linear, otherwise for $n > 1$ the effect is non-linear, and the frequencies associated to the regressive wave-like motion are monotonously increasing while the frequencies associated to the progressive wave-like motion are characterized by a minimum.

Starting from the eigenfrequencies, the eigenvectors can be addressed too. Referring to Tabs. 1 and 2 second row, in order to obtain a real-valued mode, the superposition of the two waves with $n \leq -1$ and $n \geq 1$ and the same $k$ is necessary. The resulting radial and circumferential displacements in the rotating reference system are:

$$u_{r,tot} = 2cos(n\theta + \omega_{n,1}t) + 2cos(n\theta - \omega_{n,2}t) \tag{21a}$$

$$u_{\theta,tot} = -2B_{n,1}sin(n\theta + \omega_{n,1}t) - 2B_{n,2}sin(n\theta - \omega_{n,2}t) \tag{21b}$$

In the considered range of rotating speed $\Omega$ the coefficients $B_{n,1}$ and $B_{n,2}$ are very similar to each other. By using Prostaphaeresis trigonometric formulae, Eqs. 21 can be rewritten as:

$$u_{r,tot} = 4cos\left(n\theta + \frac{\omega_{n,1} - \omega_{n,2}}{2}t\right) cos\left(\frac{\omega_{n,1} + \omega_{n,2}}{2}t\right) \tag{22a}$$

$$u_{\theta,tot} = -4B_{n,1}sin\left(n\theta + \frac{\omega_{n,1} - \omega_{n,2}}{2}t\right) cos\left(\frac{\omega_{n,1} + \omega_{n,2}}{2}t\right) \tag{22b}$$

The radial and circumferential motions have been rewritten as the product of two sinusoidal functions: the first is a wave-like function that depends on both angular position and time, while the second is a time modulating function depending only on

time. Due to the first sinusoidal function, it is evident that in this case the superposition of the two waves does not result in a standing wave.

Fig. 7 reports the radial displacement ($u_{r,tot}$) for $\Omega = 67.3$ rad/s ($V = 80$ km/h) and $n = 3$ in the rotating reference system. The pulsating behaviour of the wave is still recognisable but, by looking at the entire sequence, we can notice that the wave is rotating. The two curves representing the beginning and the end of a cycle are not superimposed as in the case $\Omega = 0$ (Fig. 5). The rotating direction depends on the speeds of the progressive and regressive waves. These are defined as:

$$c_{n,1} = \frac{\omega_{n,1}}{n} \tag{23a}$$

$$c_{n,2} = \frac{\omega_{n,2}}{n} \tag{23b}$$

where $c_{n,1}$ and $c_{n,2}$ represent the speeds of respectively the regressive and progressive wave in the rotating reference system. The speed of the superimposed wave is defined as:

$$c_{n,tot} = \frac{|\omega_{n,1} - \omega_{n,2}|}{2n} \tag{24}$$

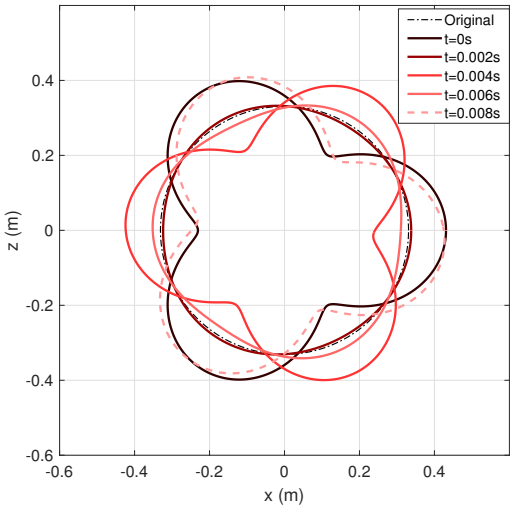


Fig. 7: Free response, ($u_{r,tot}$), of the flexible ring resulting from the superimposition of the progressive and regressive waves at $n = 3$ and $\Omega = 67.3$ rad/s ($V = 80$ km/h). Different time lapse in the rotating reference system

### 5.2 Interpretation of the Tyre Free Response in Different Reference Systems

To investigate the phenomenon highlighted in the previous section, it is possible to discuss the response in different reference systems.

A transformation can be made to move from the rotating to the absolute reference system. The relationships to move from the rotating to the absolute reference system are reported in Eq. (1), so the superimposed waves in the absolute reference system become:

$$u_{r,tot} = 2cos(n\phi + (\omega_{n,1} - n\Omega)t) + 2cos(n\phi - (\omega_{n,2} + n\Omega)t) \tag{25a}$$

$$u_{\theta,tot} = -2B_{n,1}sin(n\phi + (\omega_{n,1} - n\Omega)t) - 2B_{n,2}sin(n\phi - (\omega_{n,2} + n\Omega)t) \tag{25b}$$

The speeds of propagation respectively of the regressive and progressive waves in the absolute reference system read like:

$$c_{n,1} = \frac{|\omega_{n,1} - n\Omega|}{n} \tag{26a}$$

$$c_{n,2} = \frac{|\omega_{n,2} + n\Omega|}{n} \tag{26b}$$

This means that the regressive wave seen is slowed down in the absolute reference system, while the progressive wave is speed up. We can thus state that from the superposition of the two waves a non-standing wave is generated also in the absolute reference system. Indeed, through procedures similar to the ones described for the rotating reference system (Eq. (22)), the two superimposed waves can be written as:

$$u_{r,tot} = 4cos\left(n\phi + \frac{\omega_{n,1} - \omega_{n,2} - 2n\Omega}{2}t\right) cos\left(\frac{\omega_{n,1} + \omega_{n,2}}{2}t\right) \tag{27a}$$

$$u_{\theta,tot} = -4B_{n,1}sin\left(n\phi + \frac{\omega_{n,1} - \omega_{n,2} - 2n\Omega}{2}t\right) cos\left(\frac{\omega_{n,1} + \omega_{n,2}}{2}t\right) \tag{27b}$$

The time modulating function is the same, while the wave-like function still depends on the angular position and time. The speed of the wave-like motion component is defined as:

$$c_{n,tot} = \frac{|\omega_{n,1} - \omega_{n,2} - 2n\Omega|}{2n} \tag{28}$$

Fig. 8 shows the time radial displacement ($u_{r,tot}$) for $n = 3$ at $\Omega = 67.3$ rad/s ($V = 80$ km/h) in the absolute reference system. Again, the beginning and the ending curve of the cycle can be compared to observe the rotating effect.

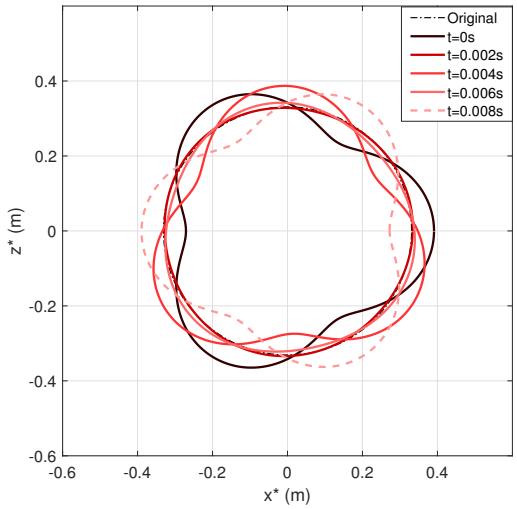


Fig. 8: Free response, ($u_{r,tot}$), of the flexible ring resulting from the superimposition of the progressive and regressive waves at $n = 3$ and $\Omega = 67.3$ rad/s ($V = 80$ km/h). Different time lapse in the absolute reference system

So, analysing the problem in the two reference systems (rotating and absolute, see Fig.1 ), we can conclude that $\Omega = 0$ results in a standing wave while for $\Omega \neq 0$ it does not. However, an alternative reference system can be identified in which the superposition of the two travelling waves gives rise to a standing wave even in the case $\Omega \neq 0$.

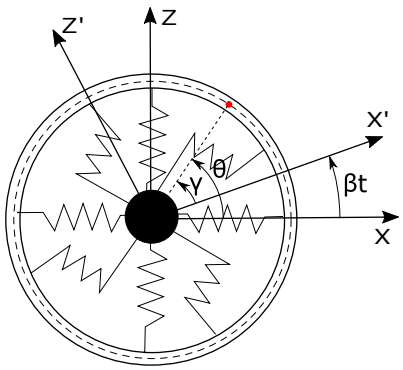


Fig. 9: Analytical model formulation of the flexible ring on elastic foundation: transformation from the rotating $(x,z)$ to the stationary $(x',z')$ reference system

To this aim, in Fig. 9 the stationary reference system $(x',z')$ is introduced. A change of coordinates is made in order to move from the rotating to the stationary frame as:

$$\theta = \gamma + \beta t \tag{29}$$

The stationary reference system is rotating with a relative speed $\beta$ that allows speeding up the slower wave ($\omega_{n,2}$) and

slowing down the faster wave ($\omega_{n,1}$). The new expressions of $u_{r,tot}$ and $u_{\theta,tot}$ in the stationary reference system become:

$$u_{r,tot} = 2cos(n\gamma + (\omega_{n,1} + n\beta)t) + 2cos(n\gamma - (\omega_{n,2} - n\beta)t) \tag{30a}$$

$$u_{\theta,tot} = -2B_{n,1}sin(n\gamma + (\omega_{n,1} + n\beta)t) - 2B_{n,2}sin(n\gamma + (\omega_{n,1} + n\beta)t) \tag{30b}$$

The speeds of propagation respectively of the regressive and progressive waves in the stationary reference system are:

$$c_{n,1} = \frac{\omega_{n,1} + n\beta}{n} \tag{31a}$$

$$c_{n,2} = \frac{\omega_{n,2} - n\beta}{n} \tag{31b}$$

By substituting in Eq. (31) the value of:

$$\beta = \frac{\omega_{n,2} - \omega_{n,1}}{2n} \tag{32}$$

the speeds of propagation become equal for the two waves ($c_n = (\omega_{n,1} + \omega_{n,2})/(2n)$), which means that their superposition gives origin to a standing wave in the stationary reference system. This effect can be seen by looking at Fig. 10.

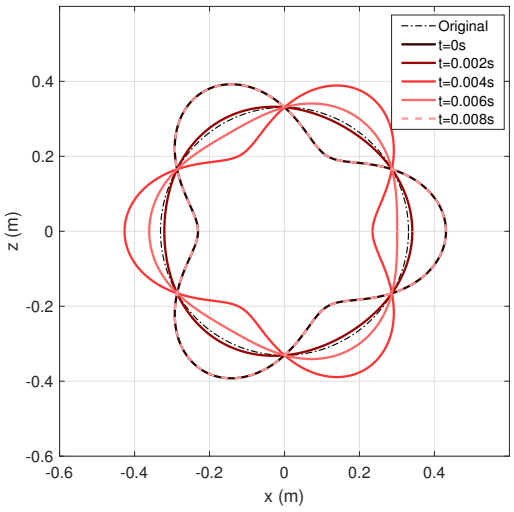


Fig. 10: Free response, ($u_{r,tot}$), of the flexible ring resulting from the superimposition of the progressive and regressive waves at $n = 3$ and $\Omega = 67.3$ rad/s ($V = 80$ km/h). Different time lapse in the stationary reference system

So, in general in the rotating case a non-standing wave is obtained unless a stationary reference system is defined. It is

worth mentioning that the stationary reference system is not unique since it changes with the order $n$ and the rotating speed.

### 5.3 The transfer inertance of the damped tyre

In the previous sections the free response of the system has been investigated in different reference systems. To deepen the comprehension of the behaviour of the tyre, the forced response should be analysed also. The PDE of motion (Eq. 6 and 7) is taken into account by adding the damping with two contributions. The first is simply given by dampers of the elastic bed in radial and circumferential directions. The second is introduced to consider the damping of the tyre material: this contribution is introduced as a loss factor in the Young Modulus, such that $E' = E(1+i\eta)$ and it is estimated through data coming from the EMA (see Section 4). Consequently, the complex values of the axial and bending stiffnesses (respectively $K'$ and $D'$) can be calculated. Tab 5 lists the damping parameters, being $c_\theta$ and $c_r$ the damping coefficients adopted for the elastic bed.

| Parameter | Value |
|---|---|
| $c_\theta$ (N s m$^{-3}$) | $1{,}5 \cdot 10^3$ |
| $c_r$ (N s m$^{-3}$) | $1{,}9 \cdot 10^3$ |
| $\eta$ ( - ) | $2{,}5 \cdot 10^{-2}$ |

Table 5: Damping parameters

To simulate the forced response of the system, an approach similar to the one proposed by Nilson in [27] for bending waves in slender rectilinear beams is considered. The equation of motion in radial direction is written only in $u_r$ exploiting a relation between $u_r$ and $u_\theta$, called *inextensional assumption* and introduced by Soedel in [18]. It states that:

$$u_r = -u'_\theta \tag{33}$$

and, together with the boundary conditions that allow the formulation of a propagative solution as described in Section 3, it provides the tools for the calculation of the forced response of the system.

Analytically, the system has been forced with a unitary impulsive force applied in a given angular position. This choice simulates a common test performed on tyres, the so-called *cleat test*. Through the passage over an obstacle the tyre is instantaneously excited while rotating and its forced response can be measured. The impulsive force also allows having a response similar to the one obtained through the EMA performed in Section 4 in the non-rotating case.

Fig. 11 shows a comparison between the experimental inertance and the analytical one for the non-rotating tyre ($\Omega = 0$ rad/s) in correspondence of the same angular position. A good matching both in terms of frequencies and amplitudes is achieved, confirming the effectiveness of the identification process of the model parameters.

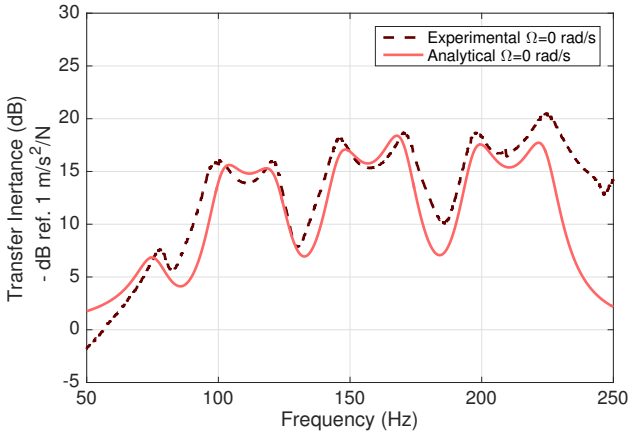


Fig. 11: Transfer Inertance between the radial force at $\Theta = 0^\circ$ and the radial acceleration at $\Theta = 100^\circ$ computed in the rotating reference system. Comparison between the FRF measured and the one simulated through the flexible ring model in non rotating conditions ($\Omega = 0$ rad/s)

When rotation is introduced ($\Omega \neq 0$ rad/s), the bifurcation effect discussed in the previous sections is expected. However, due to the high damping associated to the materials forming the tyre, there is a coupling of the different frequencies and this behaviour is not so evident (Fig. 12). The progressive and regressive waves generate a complex interaction resulting, for example in the case of study, in an increase of the peaks at low frequencies.

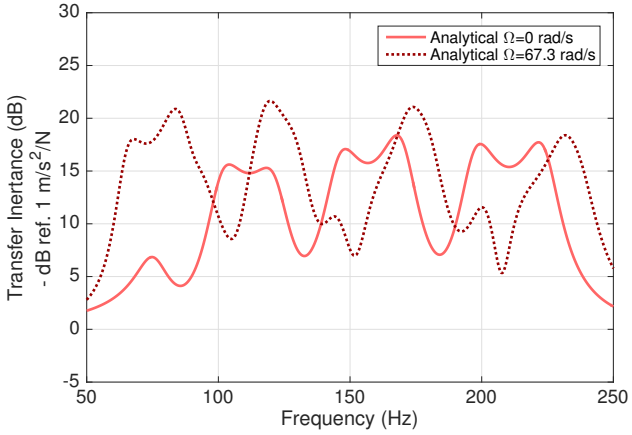


Fig. 12: Transfer Inertance between the radial force at $\Theta = 0^\circ$ and the radial acceleration at $\Theta = 100^\circ$ computed in the rotating reference system. Comparison between the FRF simulated through the flexible ring model in non rotating ($\Omega = 0$ rad/s) and rotating conditions ($\Omega = 67.3$ rad/s)

## 6 Conclusions

In this paper, we investigated the tyre-wheel system by implementing a flexible ring model suitable for studying the in-plane dynamics of the tyre. We derived the general equations of motion governing both radial and circumferential displacement of the tyre, together with the equations of motion governing the wheel dynamics. Differently from other literature models, we computed the equilibrium position due to the centrifugal load and the inflation pressure to account for the tyre

flexibility and linearised the equations of motion around it. This procedure makes the model more specific with respect to the case study (the in-plane tyre dynamics). Moreover, due to the remarkable influence of the preloads on the stiffness of the tyre-wheel system, the computation of the equilibrium position has an important role in the estimation of the tyre parameters based on experimental data.

Once the linearised equations of motion were written, we implemented the procedure for obtaining the natural frequencies and mode shapes. The model was first validated against literature data, and then a realistic set of tyre parameters were estimated through an Experimental Modal Analysis performed on a reference tyre. We investigated the effect of rotation on the system's natural frequencies (namely bifurcation). We obtained the four circular frequencies for each mode order $n$. In the non-rotating case, the circular frequencies are equal in pairs, while, when the angular speed is non null, they are different. This effect is due to the Coriolis acceleration and the increment/decrement of the circular frequencies depends on the angular speed and on the mode order considered.

As for the mode shapes, we described the procedure for realizing a real propagative wave thanks to the superposition of the $n \leq -1$ and $n \geq 1$ eigenvectors. For each mode order, we computed a progressive and a regressive wave for the inextensional and extensional cases, and investigated the stationarity of their superposition for different rotating speeds and reference systems. In the "non-rotating tyre" case, the progressive and regressive waves travel at the same speed in opposite directions, so that their superposition always results in a standing wave. When the tyre system is put in rotation, the stationarity is no longer guaranteed for both the rotating and absolute reference systems. We thus introduced the concept of a stationary reference system, which, rotating with an intermediate speed between the progressive and the regressive wave circular frequencies, allows a standing wave to be observed.

Finally, we presented a comparison between the experimental and analytical results in terms of transfer inertance for static cases, where the analytical model gives a good prediction of the tyre behaviour. We also performed a simulation for the rotating case, demonstrating how, due to the high damping of the system, the bifurcation effect is not clearly evident during the experimental cleat test.

**Acknowledgements**

This study is part of an ongoing research collaboration between Pirelli Tyre S.p.A. and Politecnico di Milano. The authors wish to thank Pirelli Tyre for its continuous support and valuable contribution to the success of this research project.

## Appendix A

The governing equations of the thin, flexible ring on elastic foundation are derived applying the Hamilton's principle.

**Energy functions**

The total kinetic energy per unit width is

$$T = T_1 + T_2 \tag{34}$$

where $T_1$ and $T_2$ are respectively the kinetic energy per unit width of the thin flexible ring and of the wheel. The first contribution can be expressed as

$$T_1 = \frac{1}{2}\int_0^{2\pi} \rho h a V^2 d\theta \tag{35}$$

The expression of the velocity $V$ of each infinitesimal arc element composing the ring is formulated as

$$V^2 = (\dot{u_r} - u_\theta\Omega)^2 + [\dot{u_\theta} + u_r\Omega + (a + u_r^o)\Omega]^2 - 2u_\theta^o\dot{u_r}\Omega + (u_\theta^o)^2\Omega^2 + 2u_\theta^o u_\theta\Omega^2 \tag{36}$$

being $\dot{\square}$ the time derivative of the considered term. Substituting equation 36 in equation 35 leads to

$$T_1 = \frac{\rho h a}{2}\int_0^{2\pi} [(\dot{u_r} - u_\theta\Omega)^2 + [\dot{u_\theta} + u_r\Omega + (a + u_r^o)\Omega]^2 - 2u_\theta^o\dot{u_r}\Omega + (u_\theta^o)^2\Omega^2 + 2u_\theta^o u_\theta\Omega^2]d\theta \tag{37}$$

The kinetic energy of the wheel ($T_2$) is given by the sum of translational and rotational terms

$$T_2 = \frac{1}{2}m(\dot{x_w^*}^2 + \dot{z_w^*}^2) + \frac{1}{2}I_r(\Omega + \dot{\theta_w})^2 \tag{38}$$

where $m$ is the mass of the wheel body and $I_r$ is the mass moment of inertia of the wheel per unit width. In order to formulate the equations of motion in the rotating reference system, a transformation of coordinates is needed. Applying relations (1) equation 38 becomes

$$T_2 = \frac{1}{2}m[(\dot{x}_w cos(\Omega t) - x_w \Omega sin(\Omega t) - \dot{z}_w sin(\Omega t) - z_w \Omega cos(\Omega t))^2 + \\ + (\dot{x}_w sin(\Omega t) + x_w \Omega cos(\Omega t) + \dot{z}_w cos(\Omega t) - z_w \Omega sin(\Omega t))^2] + \frac{1}{2} I_r (\Omega + \dot{\theta}_w)^2 \tag{39}$$

$U$ is the potential energy composed of the strain energy of the flexible ring ($U_1$) and the elastic energy of the foundation ($U_2$). To write the first contribution, the general strain-displacement relations of the flexible ring have to be derived. The three strain-displacement relations are:

- $\varepsilon_r$, the normal strain in radial direction
- $\varepsilon_\theta$, the normal strain in circumferential direction
- $\varepsilon_{r\theta}$, the in-plane shear strain

Under the Euler-Bernoulli assumption on thin rings, the cross section remains plane and normal to the middle circumference after deformation. So the only significant strain is in $\theta$ direction, while the transverse shear strain is negligible and the radial strain is null. The final expression of the strain-displacement relation in circumferential direction is

$$\varepsilon_\theta = \frac{1}{a}\left(u_r + u_r^o + u_\theta^{'} + u_\theta^{'o}\right) + \frac{s}{a^2}\left(u_\theta^{'} + u_\theta^{'o} - u_r^{''} - u_r^{''o}\right) + \frac{1}{2a^2}\left[\left(u_r + u_r^o + u_\theta^{'} + u_\theta^{'o}\right)^2 + \left(u_\theta + u_\theta^o - u_r^{'} - u_r^{'o}\right)^2\right] \tag{40}$$

where $\square^{'}$ stands for the derivatives with respect to $\theta$ and second order non linear terms in $\varepsilon_\theta$ are taken into account so as not to lose information related to the tension in the ring; $s$ is the radial distance from the middle circumference.

The strain energy per unit width of the ring can be expressed as

$$U_1 = a\int_{-h/2}^{h/2}\int_0^{2\pi}\frac{1}{2}\sigma_\theta \varepsilon_\theta d\theta dr \tag{41}$$

Hooke's low can now be introduced

$$\sigma_\theta = E\varepsilon_\theta \tag{42}$$

with E being the Young's modulus of the ring's material. By substituting equations 42 and 40 in 41 and computing the

integral over the thickness, the following expression of the strain energy is obtained

$$U_1 = \frac{1}{2}a\int_0^{2\pi}\Big[\frac{K}{a^2}(u_\theta^{'}+u_\theta^{'o}+u_r+u_r^o)^2+\frac{D}{a^4}(u_\theta^{'}+u_\theta^{'o}-u_r^{''}-u_r^{''o})^2+\frac{K}{4a^4}(u_r+u_r^o+u_\theta^{'}+u_\theta^{'o})^4+ \\ +\frac{K}{4a^4}(u_r^{'}+u_r^{'o}-u_\theta-u_\theta^o)^4+\frac{K}{a^3}(u_\theta^{'}+u_\theta^{'o}+u_r+u_r^o)^3+\frac{K}{a^3}(u_\theta^{'}+u_\theta^{'o}+u_r+u_r^o) \\ (u_r^{'}+u_r^{'o}-u_\theta-u_\theta^o)^2+\frac{K}{2a^4}(u_r+u_r^o+u_\theta^{'}+u_\theta^{'o})^2(u_r^{'}+u_r^{'o}-u_\theta-u_\theta^o)^2\Big]d\theta \tag{43}$$

where $D = E\frac{h^3}{12}$ and $K = Eh$, are respectively the bending and axial stiffness per unit width of the ring. The sidewalls of the tyre are modelled as an elastic foundation consisting of springs distributed along the entire circumference in radial and circumferential direction.

The potential energy of the elastic foundation is defined as

$$U_2 = \frac{1}{2}\int_0^{2\pi}(k_\theta\Delta l_\theta^2+k_r\Delta l_r^2)ad\theta \tag{44}$$

being $\Delta l_r$ and $\Delta l_\theta$ the elongations of the springs respectively in radial and circumferential direction and $k_r$ and $k_\theta$ the radial and circumferential stiffness ot the springs of the elastic bed. The elongations in radial and circumferential direction can be obtained as

$$\Delta l_r = u_r+u_r^o-x_w cos(\theta)-z_w sin(\theta) \tag{45a}$$

$$\Delta l_\theta = u_\theta+u_\theta^o+x_w sin(\theta)-z_w cos(\theta)-a\theta_w \tag{45b}$$

Substituting equations 45 into 44 the the final expression of the potential energy of the elastic foundation can be written as

$$U_2 = \int_0^{2\pi}[k_\theta(u_\theta+u_\theta^o+x_w sin(\theta)-z_w cos(\theta)-a\theta_w)^2+k_r(u_r+u_r^o-x_w cos(\theta)-z_w sin(\theta))^2]ad\theta \tag{46}$$

The tyre-wheel system in working conditions is subjected to forces acting at the tyre-road contact patch and at the hub. The first ones would appear in the equations of motion of the tyre, while the second ones would appear in the equations of motion of the wheel.

The tyre external forces per unit width in tangential and radial direction applied to the ring are represented by $q_\theta(t)$ and $q_r(t)$, while $p_o$ is the static contribution of the inflating pressure in radial direction. The final expression of the virtual work

per unit width of the tyre yields

$$\delta E_1 = \int_0^{2\pi} [q_\theta \delta u_\theta + (q_r + p_o)\delta u_r] a d\theta \tag{47}$$

being $\delta u_\theta$ and $\delta u_r$ the virtual displacements in circumferential and radial direction of a generic point.

Considering the reaction forces acting between the wheel and the hub, their virtual work is derived as

$$\delta E_2 = \int_0^{2\pi} f_x \delta x_w + f_z \delta z_w + T_y \delta\theta_w \tag{48}$$

where $\delta x_w$, $\delta z_w$ and $\delta\theta_w$ are the virtual displacements and rotation of the wheel and $f_x$, $f_z$ and $T_y$ represent the reaction forces and torque in the rotating reference system.

**Hamilton's principle**

The Hamilton's Principle is applied to derive the equations of motion of the tyre-wheel system. The variational form leads to

$$\delta \int_{t_1}^{t_2} \Big[ T - (U + E) \Big] dt = 0 \tag{49}$$

where $E$ is the potential energy of the external forces $(E_1 + E_2)$. By substituting the energy functions previously introduced, the integral contribution of each term is computed. Starting from equation 37, the $T_1$ contribution is

$$\begin{aligned} \int_{t_1}^{t_2} \delta T_1 dt = \rho h a \int_{t_1}^{t_2} dt \int_0^{2\pi} \Big[ & (\dot{u}_r - u_\theta \Omega)(\delta \dot{u}_r - \delta u_\theta \Omega) + [\dot{u}_\theta + u_r \Omega + (a + u_r^o)\Omega](\delta \dot{u}_\theta + \delta u_r \Omega) + \\ & - u_\theta^o \Omega \delta \dot{u}_r + u_\theta^o \Omega^2 \delta u_\theta \Big] d\theta \\ = \rho h a \int_{t_1}^{t_2} dt \int_0^{2\pi} \Big[ & [\dot{u}_\theta \Omega + u_r \Omega^2 + (a + u_r^o)\Omega^2]\delta u_r + (-\Omega \dot{u}_r + u_\theta \Omega^2 + u_\theta^o \Omega^2)\delta u_\theta + \\ & + (\dot{u}_r - u_\theta \Omega - u_\theta^o \Omega)\delta \dot{u}_r + [\dot{u}_\theta + u_r \Omega + (a + u_r^o)\Omega]\delta \dot{u}_\theta \Big] d\theta \end{aligned} \tag{50}$$

The last two parenthesis are multiplied by $\delta\dot{u}_\theta$ and $\delta\dot{u}_r$ which are the time derivatives of the virtual displacements. Integration by parts of these terms has been performed to reconduct them to be dependent on the virtual displacement $\delta u_r$ and $\delta u_\theta$

$$\int_{t_1}^{t_2}(\dot{u}_r - u_\theta\Omega - u_\theta^o\Omega)\delta\dot{u}_r dt = (\dot{u}_r - u_\theta\Omega - u_\theta^o\Omega)\delta u_r\Big|_{t_1}^{t_2} - \int_{t_1}^{t_2}(\ddot{u}_r - \dot{u}_\theta\Omega)\delta u_r \tag{51}$$

$$\int_{t_1}^{t_2}[\dot{u}_\theta + u_r\Omega + (a+u_r^o)\Omega]\delta\dot{u}_\theta dt = [\dot{u}_\theta + u_r\Omega + (a+u_r^o)\Omega]\delta u_\theta\Big|_{t_1}^{t_2} - \int_{t_1}^{t_2}(\ddot{u}_\theta + \dot{u}_r\Omega)\delta u_\theta dt \tag{52}$$

In both cases, from the integration by parts two terms appear: the first ones are equal to zero because of the assumption that the virtual displacement is zero at $t = t_1$ and $t = t_2$; the second ones have to be inserted in equation 51. Combining equations 51 and 52 with 50 and putting in evidence the terms multiplying $\delta u_\theta$ and $\delta u_r$, the final expression of the kinetic energy $T_1$ is obtained

$$\begin{aligned}\int_{t_1}^{t_2}\delta T_1 dt = \int_{t_1}^{t_2} dt\rho ha\int_0^{2\pi}\Big[&[-\ddot{u}_r + 2\dot{u}_\theta\Omega + u_r\Omega^2 + (a+u_r^o)\Omega^2]\delta u_r + \\ &+ [-\ddot{u}_\theta - 2\dot{u}_r\Omega + (u_\theta + u_\theta^o)\Omega^2]\delta u_\theta\Big]d\theta\end{aligned} \tag{53}$$

The first term is the one belonging to the equation of motion in the radial direction while the second one belongs to the equation of motion in the circumferential direction.

As concerns $T_2$, it generates contributions to the equations of motion of the wheel.

$$\int_{t_1}^{t_2}\delta T_2 dt = \Big[-m(-\ddot{x}_w + 2\dot{z}_w\Omega + x_w\Omega^2)\Big]\delta x_w + \Big[-m(-\ddot{z}_w - 2\dot{x}_w\Omega + z_w\Omega^2)\Big]\delta z_w + I_r\ddot{\theta}_w\delta\theta_w \tag{54}$$

Applying a similar procedure to the potential energies $U + E$, we obtain

$$
\begin{aligned}
\int_{t_1}^{t_2}\delta(U+E)dt = &\left[(u_r^o)^3\left(\frac{K}{2a^4}\right)+(u_r^o)^2\left(\frac{3K}{2a^3}\right)+(u_\theta^o)^2\left(\frac{K}{2a^3}\right)+u_r^o(u_\theta^o)^2\left(\frac{K}{2a^4}\right)+u_r^o\left(k_r+\frac{K}{a^2}\right)-p_o+\right.\\
&+\frac{K}{a^2}(u_\theta^{'}+u_r)+\frac{D}{a^4}(u_r^{IV}-u_\theta^{'''})+\frac{K}{2a^4}(u_r^o)^2(3u_r+4u_\theta^{'}-u_r^{''})+\frac{K}{a^3}u_r^o(3u_r+4u_\theta^{'}-u_r^{''})+\\
&\left.+k_r(u_r-x_w cos\theta-z_w sin\theta)-q_r\right]\delta u_r+\left[(u_\theta^o)^3\left(\frac{K}{2a^4}\right)+(u_r^o)^2u_\theta^o\left(\frac{K}{2a^4}\right)+u_r^o u_\theta^o\left(\frac{K}{a^3}\right)+u_\theta^o(k_\theta)+\right.\\
&-\frac{K}{a^2}(u_\theta^{''}+u_r^{'})-\frac{D}{a^4}(u_\theta^{''}-u_r^{'''})-\frac{K}{2a^4}(u_r^o)^2(-u_\theta+4u_r^{'}+3u_\theta^{''})-\frac{K}{a^3}u_r^o(-u_\theta+4u_r^{'}+3u_\theta^{''})+\\
&\left.+k_\theta(u_\theta+x_w sin\theta-z_w cos\theta-a\theta_w)-q_\theta\right]\delta u_\theta+\\
&+\left[a\pi(k_\theta+k_r)x_w+a\int_0^{2\pi}[k_\theta u_\theta sin\theta-k_r u_r cos\theta]d\theta-f_x\right]\delta x_w+\\
&+\left[a\pi(k_\theta+k_r)z_w+a\int_0^{2\pi}[-k_\theta u_\theta cos\theta-k_r u_r sin\theta]d\theta-f_z\right]\delta z_w+\\
&+\left[2\pi k_\theta a^3\theta_w-a^2\int_0^{2\pi}k_\theta u_\theta d\theta-T_y\right]\delta\theta_w
\end{aligned}
\tag{55}
$$

**References**


[1] BERNARD, R. and WAYSON, R. (2005). *An introduction to Tire/Pavement Noise of Asphalt Pavement*. Institute for Safe, Quiet and Durable Highways, Purdue University

[2] MARBJERG, G. (2013). *Noise from electric vehicles - a literature survey Nr. 537*. Vejdirectoratet

[3] HARRISON, M. (2004). *Vehicle Refinement: Controlling Noise and Vibration in Road Vehicles*. SAE International, Oxford, UK.

[4] PANG, J. (2018). *Noise and Vibration Control in Automotive Bodies* Chine Machine Press, John Wiley & Sons

[5] WANG, X. and MOHAMED, Z. (2016). *A deterministic and statistical energy analysis of tyre cavity resonance noise*. Mechanical Systems and Signal Processing, 70-71, pp. 947-957.

[6] WANG, X. and MOHAMED, Z. (2015). *A study of tyre cavity resonance and noise reduction using inner trim*.Mechanical Systems and Signal Processing, 50-51, pp. 498-509.

[7] BOLTON, J.S. and CAO, R. (2015). *Improved Model for Coupled Structural-Acoustic Modes of Tires*. SAE International Journal of Passenger Cars - Mechanical Systems, 8 (3), pp. 845-854.

[8] BOLTON, J.S. and JESSOP, A.M. (2011). *Tire surface vibration and sound radiation resulting from the tire cavity mode*. Tire Science and Technology, 39 (4), pp. 245-255.

[9] BARO, S., CORRADI, R., ABOM, M., CARACINO, P. and FIORAVANTI, A.P. (2019). *Modelling of a lined tyre for predicting cavity noise mitigation*. Applied Acoustics, 155, pp. 391-400.

[10] PERISSE, J. (2002). *A study of radial vibrations of a rolling tyre for tyre-road noise characterisation* Mechanical Systems and Signal Processing, 16 (6), pp. 1043-1058.

[11] DIAZ, C.G, KINDT, P., MIDDELBERG, L., VERCAMMEN, S., THIRY, C., CLOSE, R. and LEYSSENS, J. (2016). *Dynamic behaviour of a rolling tyre: Experimental and numerical analyses*. Journal of Sound and Vibration 364, pp. 147-164

[12] GONG, S. (1993). *A study of In-Plane Dynamics of Tires*. Doctorate Thesis, Delft University of Technology

[13] LOPEZ, I., BLOM, R.E.A., ROOZEN, N.B. and NIJMEIJER, H. (2007). *Modeling the vibrations of a rotating tyre: a modal approach*. Journal of Sound and Vibrations n. 307, pp. 481-494

[14] NACKENHORST, U. (2004). *The ALE-formulation of bodies in rolling contact-Theoretical foundations and finite element approach*. Computational Methods Applied Mechanics Engineering 193, pp. 4299-4322

[15] ENDO, M., HATAMURA, K., SAKATA, M. and TANIGUCHI, O. (1984). *Flexural Vibration of a thin rotating ring*. Journal of Sound and Vibrations, n. 92(2),pp. 261-272

[16] PINNINGTON, R.J. and BRISCOE, A.R.(2001). *A wave model for a pneumatic tyre belt*. Journal of Sound and Vibration 253(5), pp. 941-959

[17] SOEDEL, W. (1975). *On the dynamic response of rolling tires according to thin shell approximation*. Journal of Sound and Vibrations n. 41(2), pp. 233-246

[18] SOEDEL, W. (2004). *Vibrations of Shells and Plates-Third edition, Revised and Explained*. Marcel Dekker, New York, chapter 4,6,16

[19] HUANG, S. C. and SOEDEL, W. (1987). *Effect of Coriolis acceleration on the free and forced in-plane vibrations of rotating rings on elastic foundation*. Journal of Sound and Vibrations, n. 115(2), pp. 253-274

[20] KINDT, P., SAS, P. and DESMET, W. (2009). *Development and validation of a three-dimensional ring-based structural tyre model*. Journal of Sound and Vibrations, 326 3-52), pp. 852-868

[21] LU, T.,TSOUVALAS, A. and METRIKINE, A.V. (2017). *The in-plane free vibration of an elastically supported thin ring rotating at high speeds revisited*. Journal of Sound and Vibrations, n. 402,pp. 203-218

[22] LIN, J. and SOEDEL, W. (1988). *On general in-plane vibrations of rotating thick and thin rings*. Journal of Sound and Vibrations, n. 122(3),pp. 547-570

[23] LIN, J. and SOEDEL, W. (1988). *On the critical speeds of rotating thick or thin rings*. Mechanics of Structures and Machines, n. 16(4),pp. 439-483

[24] GONG, S.,SAVKOOR, R. and PACEJKA, H. (1993). *The Influence of Boundary Conditions on the Vibration Transmission Properties of Tires*. SAE International, USA

[25] COOLEY, C.G.,PARKER, R.G. (2014). *Vibration of high-speed rotating rings coupled to space-fixed stiffnesses*. Journal of Sound and Vibrations, n. 333,pp. 2631-2648

[26] LU, T.,TSOUVALAS, A. and METRIKINE, A.V. (2019). *A high-order model for in-plane vibrations of rotating rings on elastic foundation*. Journal of Sound and Vibrations, n. 455,pp. 118-135

[27] NILSSON, A. and LIU, B.(2016). *Vibro-Acoustics*. Science Press, Beijing and Springer-Verlag Berlin Heidelberg

[28] HEYLEN, W., LAMMENS, S. and SAS, P. (1998). *Modal analysis theory and testing*. Katholieke Universiteit Leuven, Faculty of Engineering, Dept. of Mechanical Engineering, Division of Production Engineering, Machine Design and

Automation

[29] VAN DER AUWERAER, H., GUILLAUME, P., VERBOVEN, P. and VANLANDUIT, S. (2001). *Application of a fast-stabilizing frequency domain parameter estimation method*. ASME. J. Dyn. Sys., Meas., Control. 123(4): 651–658

**List of Figures**

**List of Tables**